

# Magnetohydrodynamic Effects in Propagating Relativistic Jets: Reverse Shock and Magnetic Acceleration

Yosuke Mizuno<sup>1,2</sup>, Bing Zhang<sup>2</sup>, Bruno Giacomazzo<sup>3</sup>, Ken-Ichi Nishikawa<sup>1</sup>, Philip E. Hardee<sup>4</sup>, Shigehiro Nagataki<sup>5</sup>, Dieter H. Hartmann<sup>6</sup>

## ABSTRACT

We solve the Riemann problem for the deceleration of an arbitrarily magnetized relativistic flow injected into a static unmagnetized medium in one dimension. We find that for the same initial Lorentz factor, the reverse shock becomes progressively weaker with increasing magnetization  $\sigma$  (the Poynting-to-kinetic energy flux ratio), and the shock becomes a rarefaction wave when  $\sigma$  exceeds a critical value,  $\sigma_c$ , defined by the balance between the magnetic pressure in the flow and the thermal pressure in the forward shock. In the rarefaction wave regime, we find that the rarefied region is accelerated to a Lorentz factor that is significantly larger than the initial value. This acceleration mechanism is due to the strong magnetic pressure in the flow. We discuss the implications of these results for models of gamma-ray bursts and active galactic nuclei.

*Subject headings:* active galactic nuclei; gamma-rays: bursts – numerical – MHD – relativity

## 1. Introduction

Relativistic jets are believed to exist in active galactic nuclei (AGNs), black hole binaries, and gamma-ray bursts (GRBs). The composition of these jets is poorly understood. It has

---

<sup>1</sup>Center for Space Plasma and Aeronomic Research, University of Alabama in Huntsville, NSSTC, 320 Sparkman Drive, Huntsville, AL 35805, USA; mizuno@cspar.uah.edu.

<sup>2</sup>Department of Physics and Astronomy, University of Nevada, Las Vegas, NV 89154, USA.

<sup>3</sup>Max-Planck-Institut für Gravitationsphysik, Albert-Einstein-Institut, Potsdam-Golm, Germany.

<sup>4</sup>Department of Physics and Astronomy, University of Alabama, Tuscaloosa, AL 35487, USA.

<sup>5</sup>Yukawa Institute for Theoretical Physics, Kyoto University, Sakyo, Kyoto, Japan.

<sup>6</sup>Department of Physics and Astronomy, Clemson University, Clemson, SC 29634, USA.

been widely argued that magnetic fields play an important role in these jets (e.g. Lovelace 1976; Blandford 1976; Blandford & Znajek 1977; Blandford & Payne 1982; Usov 1992; Thompson 1994; Mészáros & Rees 1997; Lyutikov & Blandford 2003; Vlahakis & Königl 2003, 2004), but the degree of magnetization, usually quantified by the magnetization parameter  $\sigma$  (the ratio of the electromagnetic to the kinetic energy flux), is poorly constrained by observations. GRB afterglow modeling indicates that the ejecta are more magnetized than the ambient medium, suggesting a possibly important role for magnetic fields in launching the GRB jets (Fan et al. 2002; Zhang, Kobayashi & Mészáros 2003; Kumar & Panaitescu 2003; Gomboc et al. 2008).

One possible diagnostic for the degree of magnetization in the jet is through studying the interaction between the decelerating jet and the ambient medium. The addition of magnetic field pressure in the jet alters the condition for formation of a reverse shock (RS) as well as the strength of the RS (Kennel & Coroniti 1984). Analytical studies of the deceleration of a GRB fireball with arbitrary magnetization (Zhang & Kobayashi 2005, hereafter ZK05; see also Fan et al. 2004 for  $\sigma \leq 1$ ) suggest some novel behavior that does not exist in pure hydrodynamic (HD) ( $\sigma = 0$ ) models (Sari & Piran 1995; Kobayashi et al. 1999). However, a consensus as to the conditions required for the existence of the RS or how Poynting flux is transferred to kinetic flux in the interaction region has not yet been achieved (ZK05; Lyutikov 2006; Giannios et al. 2008).

In this Letter, we present a one-dimensional (1-D) study of the interaction between a magnetized relativistic flow and an unmagnetized external medium. A Riemann problem is solved both analytically and numerically over a broad range of  $\sigma$ .

## 2. The Riemann Problem

We consider a Riemann problem consisting of two uniform initial states (left and right) with discontinuous hydrodynamic properties specified by the rest-mass density  $\rho$ , gas pressure  $p$ , specific internal energy  $u$ , specific enthalpy  $h \equiv 1 + u/\rho c^2 + p/\rho c^2$ , and normal velocity  $v^N$ . The right state (the medium external to the jet) is assumed to be a cold fluid with constant density, at rest. Specifically, we select the following initial conditions:  $\rho_R = 1.0\rho_0$ ,  $p_R = 10^{-2}\rho_0 c^2$ ,  $v_R^N = v_R^x = 0.0$ , where  $\rho_0$  is an arbitrary normalization constant (our simulations are scale-free) and  $c$  is the speed of light in vacuum. The left state (the propagating relativistic flow) is assumed to have a higher density and pressure than the right state, as well as a relativistic velocity. Specifically,  $\rho_L = 10^2\rho_0$ ,  $p_L = 1.0\rho_0 c^2$ , and  $v_L^N = v_L^x = 0.995c$  ( $\gamma_L \simeq 10$ ). The fluid is described by an adiabatic equation of state  $p \propto \rho^\Gamma$  with  $\Gamma = 4/3$ .

To investigate the effects of magnetic fields, we consider a perpendicular field component in the jet with  $B^y = 31.623, 100.0, 316.23$ , and  $447.21$  in units of  $(4\pi\rho_0 c^2)^{1/2}$  measured in the laboratory frame. This corresponds to  $\sigma \equiv B^2/4\pi\gamma^2 h\rho c^2 \simeq B^2/4\pi\gamma^2 \rho c^2$  being  $0.1, 1.0, 10.0$ , and  $20.0$ , respectively. The perpendicular field is motivated by the likely toroidal field domination at the deceleration radius for GRB outflows (e.g., Spruit et al. 2001; ZK05). In this setting, increasing  $\sigma$  increases the total (kinetic plus magnetic) energy density of the left (jet) state.

### 3. Results

We calculate exact solutions of this problem, using the code of Giacomazzo & Rezzolla (2006), in the region  $0.8 \leq x \leq 1.2$  with an initial discontinuity at  $x = 1.0$ , where  $x$  is in arbitrary units.

#### 3.1. Flow-Medium Interaction

The exact solutions are presented in Figure 1. The four panels display profiles of the gas density, the gas (and magnetic) pressure, the magnetic field strength  $B^y$ , and the Lorentz factor at time  $t = 0.16$ <sup>1</sup>. Different colors represent different  $\sigma$  values:  $0.1$  (black),  $1.0$  (red),  $2.7$  (yellow),  $10.0$  (green) and  $20.0$  (blue). The initial Lorentz factor of the left state (jet) is  $\gamma_L = 10$ .

For  $\sigma = 0.1$  (black), the solution shows a right-moving fast shock (forward shock;  $S_{\rightarrow}$ ), a left-moving fast shock (reverse shock;  $\leftarrow S$ ) and a fixed contact discontinuity ( $C$ ) in the rest frame of the contact discontinuity. In the laboratory frame, the contact discontinuity and the two shocks all move to the right.

For  $\sigma = 1.0$  (red), the solution shows similar profiles ( $\leftarrow SCS_{\rightarrow}$ ) as for  $\sigma = 0.1$ . The forward shock is stronger (due to a higher pressure discontinuity) and slower (more deceleration relative to the frame of the contact discontinuity), while the reverse shock is weaker and propagating faster than in the case of  $\sigma = 0.1$ . These features are expected from the analytical work of ZK05 and Giannios et al. (2008), and also agree with the 1-D relativistic MHD simulations of Mimica et al. (2007, 2008).

When the magnetization of the flow becomes stronger than  $\sigma = 2.7$ , the shock profiles

---

<sup>1</sup>Here  $t$  is in units of  $x/c$  with  $c = 1$ .

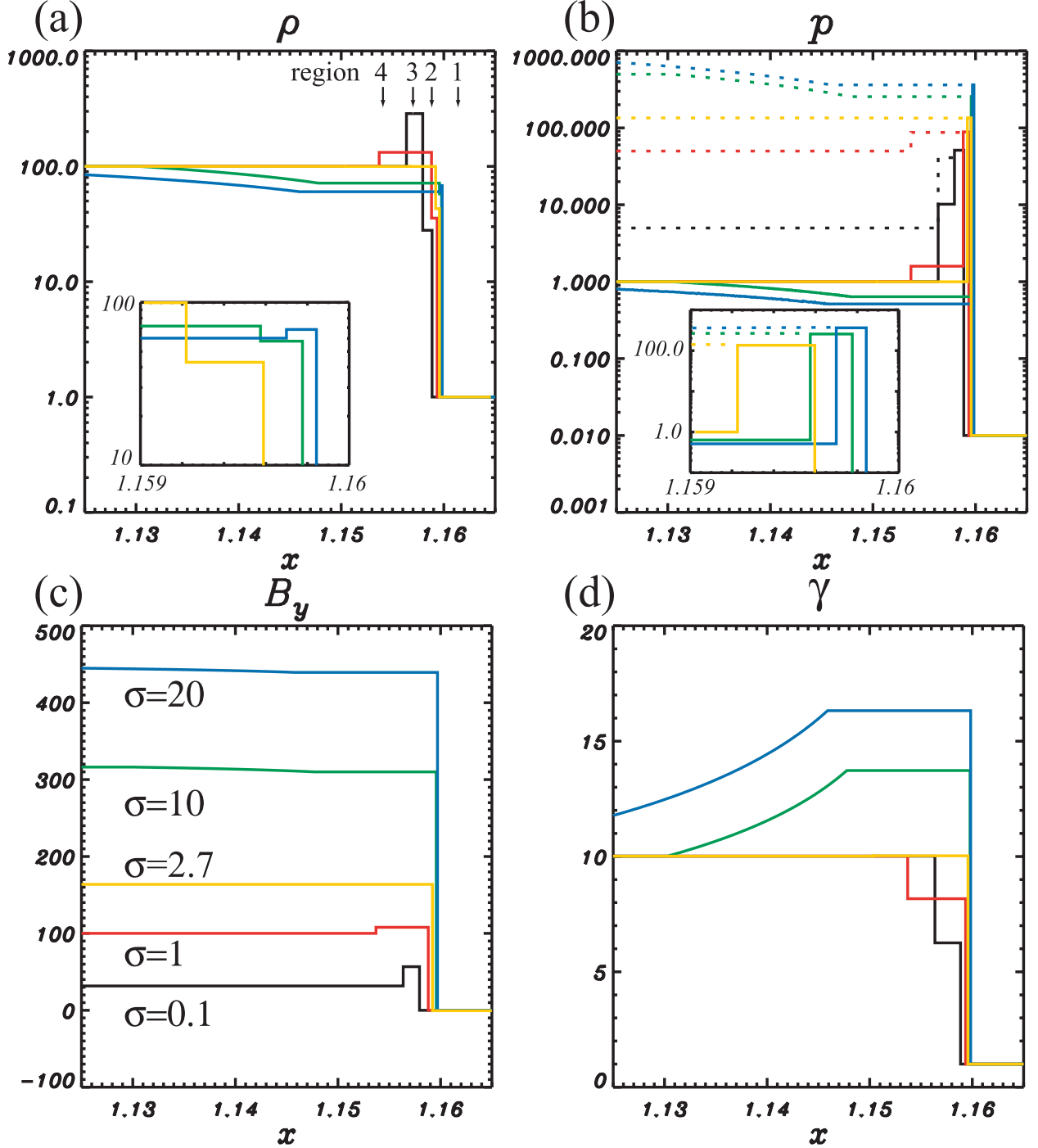


Fig. 1.— Profiles of (a) density, (b) gas pressure (*solid lines*) and magnetic pressure (*dotted lines*), (c) magnetic field ( $B_y$ ), and (d) Lorentz factor ( $\gamma$ ) of  $\sigma = 0.1$  (black), 1.0 (red), 10.0 (green), 20.0 (blue) cases at time  $t = 0.16$ . Other parameters:  $\rho_L = 100.0$ ,  $\rho_R = 1.0$ ,  $\gamma_L = 10.0$ . The critical value,  $\sigma_c \simeq 2.7$  case is shown as yellow lines. Close-up forward shock regions are inserted. Arrows indicate four physically distinct regions: (1) unshocked medium, (2) shocked medium, (3) shocked flow and (4) unshocked flow corresponding to the  $\sigma = 0.1$  case.

change drastically (the significance of this particular  $\sigma$  value is discussed below). For  $\sigma = 10.0$  (green) and  $\sigma = 20.0$  (blue), a prominent left-going rarefaction wave ( $\leftarrow R$ ) is observed, instead of a left-going shock (see also Romero et al. 2005; Mimica et al. 2007). When the rarefaction wave propagates into the jet flow, density and gas pressure in the flow decrease, and the flow velocity increases. The terminal Lorentz factor of the left (jet) state and the forward shock region reaches  $\gamma \sim 14$  for  $\sigma = 10$  and  $\gamma > 16$  for  $\sigma = 20$ . This *magnetic acceleration* mechanism stems from the magnetic pressure in the flow<sup>2</sup>.

This magnetic acceleration mechanism is a pure MHD effect and requires the magnetic field to generate a rarefaction wave. This is a very different mechanism from the HD/MHD boost mechanism proposed by Aloy & Rezzolla (2006), and further investigated by Mizuno et al. (2008) and Aloy & Mimica (2008). The HD/MHD mechanism is a purely relativistic mechanism, which invokes a relativistic flow that is perpendicular to the propagation direction of the rarefaction wave. The mechanism discussed here occurs even in the Newtonian case, and acts parallel to the propagation direction of the rarefaction wave. In general, the acceleration efficiency is smaller than that of the HD/MHD boost mechanism (see §3.3 for more discussions).

### 3.2. Physical Conditions for Reverse Shock or Magnetic Acceleration

The magnetic pressure profiles (dotted lines) in Fig. 1(b) reveal the physical condition required for the transition from a reverse shock to a rarefaction wave. It is evident that the magnetic pressure increases as  $\sigma$  increases. In the reverse shock cases ( $\sigma = 0.1, 1$ ), the upstream magnetic pressure is lower than the gas pressure in the forward shock, while in the rarefaction wave cases ( $\sigma = 10, 20$ ), the upstream magnetic pressure exceeds the gas pressure in the forward shock. Thus, the balance between the upstream magnetic pressure in the unshocked flow region and the forward shock gas pressure in the shocked medium (ZK05; Romero et al. 2005) provides the physical condition that separates the two regimes.

This condition can be derived analytically (see also ZK05). For the interaction between a relativistic flow and an external medium, there are four physically distinct regions: (1) unshocked medium, (2) shocked medium, (3) shocked flow, and (4) unshocked flow. Hereafter,  $Q_i$  denotes the value of a quantity “ $Q$ ” in region “ $i$ ”. Based on the relativistic shock jump conditions with  $\Gamma = 4/3$ , one can write  $u_2/\rho_2 c^2 = (\gamma_2 - 1) \simeq \gamma_2$  and  $\rho_2/\rho_1 = 4\gamma_2 + 3 \simeq 4\gamma_2$ .

---

<sup>2</sup>We note that Romero et al. (2005) and Mimica et al. (2007) also discovered the rarefaction wave regime discussed in this paper, but did not investigate the magnetic acceleration mechanism and its astrophysical implications in detail.

A constant speed across the contact discontinuity requires  $\gamma_2 = \gamma_3$ , and the relation between the gas pressure and the internal energy gives  $p_2 = u_2/3$ . Thus, the thermal pressure generated in the forward shock region is  $p_2 = (1/3)(\gamma_2 - 1)(4\gamma_2 + 3)\rho_1 c^2 \simeq (4/3)\gamma_2^2 \rho_1 c^2$ . The pressure balance condition can be written as  $B_4^2/8\pi\gamma_4^2 \sim p_2$ . This is because at pressure balance there is no reverse shock or rarefaction wave, so that region 4 and region 3 are matched as  $B_4 \simeq B_3$ , and  $\gamma_4 \simeq \gamma_3 = \gamma_2$ . Using the definition of  $\sigma \equiv \sigma_4 = B_4^2/4\pi\gamma_4^2\rho_4 c^2$ , one can derive a critical  $\sigma_c$  value

$$\sigma_c = \frac{2}{3}(\gamma_4 - 1)(4\gamma_4 + 3)\frac{\rho_1}{\rho_4} \simeq \frac{8}{3}\gamma_4^2\frac{\rho_1}{\rho_4} = \frac{8}{3}\gamma_L^2\frac{\rho_R}{\rho_L}. \quad (1)$$

The condition for the existence of a reverse shock is  $\sigma < \sigma_c$ , which is Eq. (31) of ZK05. The condition for a rarefaction wave and magnetic acceleration is  $\sigma > \sigma_c$ . In our calculation, we adopted  $\rho_1 = \rho_R = 1.0$ ,  $\rho_4 = \rho_L = 10^2$ , and  $\gamma_4 = \gamma_L = 10.0$ . The critical value becomes  $\sigma_c \simeq 2.7$ . Our calculations indicate that  $\sigma_c$  marks the transition point where neither a reverse shock nor a rarefaction wave is established (see yellow lines in Fig. 1).

To verify this critical condition in a larger parameter space, we investigate the  $\sigma$ -dependences of various quantities in detail. In Fig. 2(a), we plot the gas pressure in the region through which the reverse shock/rarefaction wave has propagated. The initial Lorentz factor is taken as  $\gamma_L = 5, 10$ , and  $20$ , respectively. For all the cases, we fix a constant flow density at  $\rho_L = 10^2$  and increase  $B$  (hence  $\sigma$ ). The total initial energy density of the flow increases with  $\sigma$ . In all cases, the gas pressure decreases with  $\sigma$  smoothly without a sharp transition from the RS regime (denoted by solid lines) to the reverse rarefaction wave regime (denoted by dotted lines). The critical magnetization parameters are  $\sigma_c \simeq 0.7, 2.7, 10.6$  for  $\gamma_L = 5, 10, 20$ , respectively, derived from the analytical solution Eq.(1). We notice that in the reverse shock regime, the strength of the shock decreases rapidly with increasing  $\sigma$ . The critical magnetization parameter  $\sigma_c$  increases with  $\gamma_L$ , so that a RS can exist in the high- $\sigma$  regime if  $\gamma_L$  is sufficiently large (see also ZK05).

Another commonly invoked condition for a reverse shock is that the shock speed in the fluid frame (region 4) is higher than the speed of the Alfvén wave, i.e.  $\gamma'_{\text{RS,RR}} > \gamma'_A$ , where  $\gamma'_{\text{RS,RR}} = (\gamma_4/\gamma_{\text{RR,RS}} + \gamma_{\text{RR,RS}}/\gamma_4)/2$ ,  $\gamma'_A = (1 + \sigma)^{1/2}$ , and  $\gamma_{\text{RS,RR}}$  is the Lorentz factor of the reverse shock or reverse rarefaction wave in the laboratory frame, which can be calculated using the exact solution of Giacomazzo & Rezzolla (2006). Some authors (Giannios et al. 2008) claimed that this condition is different from the pressure balance condition. In Figures 2(b) and 2(c), we present the ratios of gas pressure in the forward shock region to magnetic pressure in the flow,  $p_{\text{FS}}/p_B$ , and  $\gamma'_{\text{RS,RR}}/\gamma_A$ , and find that both ratios reach unity at the same critical value  $\sigma_c$ . This suggests that the two reverse shock conditions have intrinsically the same physical origin, at least for the 1D model we are studying.

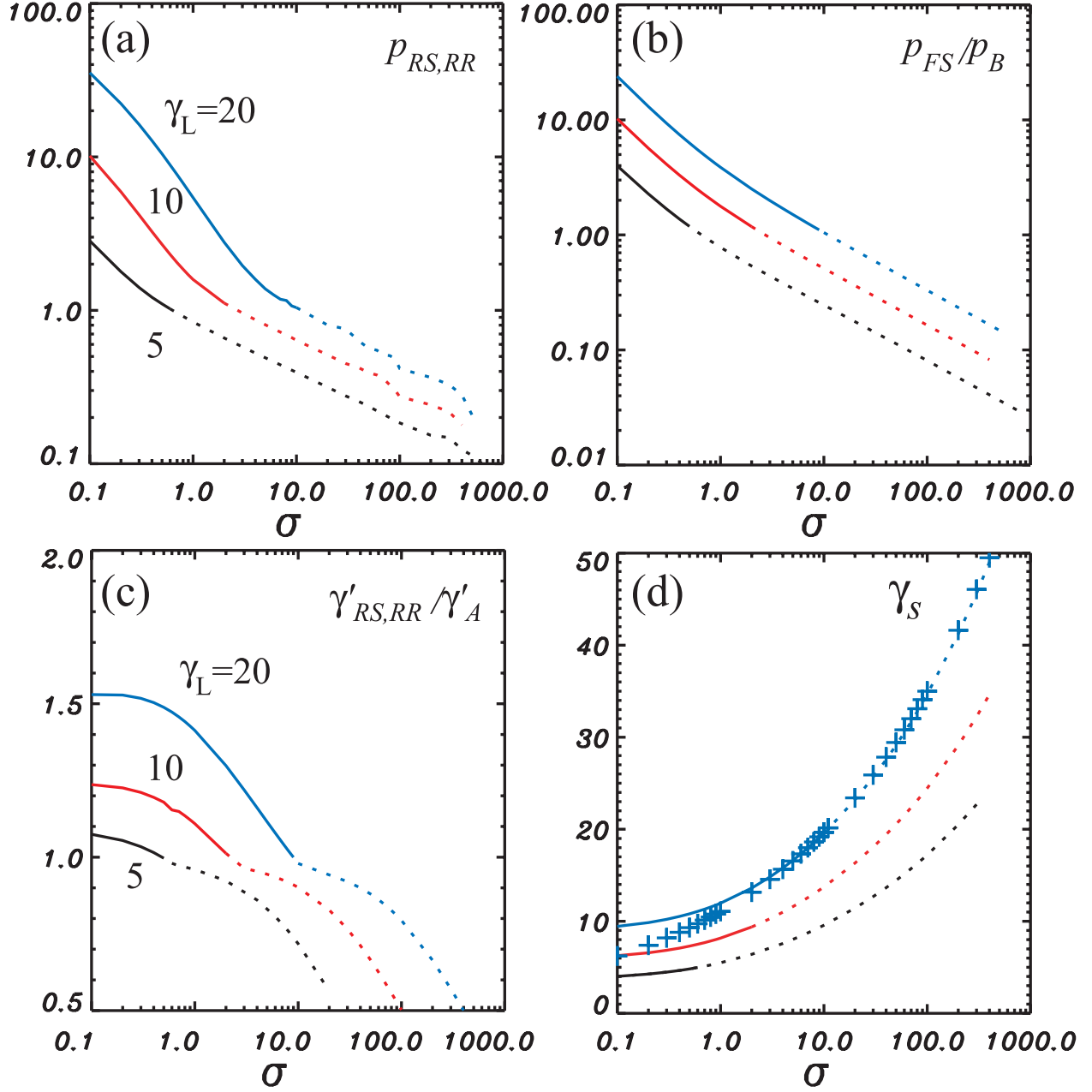


Fig. 2.— The  $\sigma$ -dependences of (a) gas pressure in the region through which the reverse shock (RS; solid lines)/rarefaction wave (RR; dotted lines) has propagated; (b) the ratio of the gas pressure in the forward shock region to the magnetic pressure in the flow; (c) the ratio of the Lorentz factor of the propagating reverse shock/rarefaction wave to the Alfvén Lorentz factor in the rest frame of the fluid; (d) the maximum Lorentz factor in the shocked region, in the exact solution. Different initial Lorentz factors have been calculated:  $\gamma_L = 5$  (black), 10 (red), and 20 (blue). Crosses are the values of the estimated terminal Lorentz factor in the  $\gamma_L = 20$  case according to Eq.(2). A constant flow density is adopted, so that the total initial energy density of the flow increases with  $\sigma$ .

### 3.3. Terminal Lorentz Factor and Magnetic Acceleration Efficiency

To understand the magnetic acceleration mechanism better, we plot the Lorentz factor as a function of  $\sigma$  in Fig. 2(d). For the magnetic acceleration case, this is the terminal Lorentz factor after acceleration. Because of the dependence of  $\sigma_c$  on  $\gamma_L$ , a higher  $\sigma$  is needed to achieve acceleration for a higher  $\gamma_L$ .

The terminal Lorentz factor can be estimated analytically by requiring that the thermal pressure in the forward shock region balances the magnetic pressure in the region through which the rarefaction wave has propagated. For terminal Lorentz factor  $\gamma_t$ , this condition can be roughly expressed as  $B_3^2/8\pi\gamma_t^2 = (1/3)(\gamma_t - 1)(4\gamma_t + 3)\rho_1 c^2 \simeq (4/3)\gamma_t^2 \rho_1 c^2$ . Using the definition of  $\sigma$  with  $B_4 \simeq B_3$ , this condition becomes

$$\gamma_t \simeq \left( \frac{3\gamma_4^2 \sigma \rho_4}{8\rho_1} \right)^{1/4}. \quad (2)$$

Crosses in Fig.2(d) denote the values of terminal Lorentz factors calculated from Eq.(2) for our model parameters,  $\gamma_4 = \gamma_L = 20$ ,  $\rho_1 = \rho_R = 1.0$ , and  $\rho_4 = \rho_L = 10^2$ . This is in good agreement with the exact solution of the Riemann problem in the reverse rarefaction wave regime.

To investigate the acceleration efficiency, we present the terminal Lorentz factor  $\gamma_t$ , and the ratio between the terminal Lorentz factor and the initial Lorentz factor ( $\gamma_t/\gamma_L$ ) as a function of the initial flow Lorentz factor  $\gamma_L$  in Fig. 3. While a flow with a higher initial Lorentz factor reaches a higher terminal Lorentz factor, that with a lower initial Lorentz factor experiences a higher acceleration efficiency. From Eq.(2) it is straightforward to show that the acceleration efficiency  $\gamma_t/\gamma_4 \simeq (3\sigma\rho_4/8\rho_1)^{1/4}\gamma_4^{-1/2}$ . This is in good agreement with the exact solution of the Riemann problem in relativistic regime.

## 4. Summary and Discussion

We solved the 1-D Riemann problem for the deceleration of an arbitrarily magnetized relativistic flow in a static unmagnetized medium. For the same initial Lorentz factor, the reverse shock becomes progressively weaker with increasing  $\sigma$ . It turns into a rarefaction wave when  $\sigma$  exceeds a critical value,  $\sigma_c$ , at which point the magnetic pressure in the flow is balanced by the thermal pressure in the forward shock. In the rarefaction wave regime, material in the forward shock region is accelerated due to the strong magnetic pressure in the flow. This magnetic acceleration mechanism may thus play an important role in the dynamics of strongly magnetized, relativistic flows.



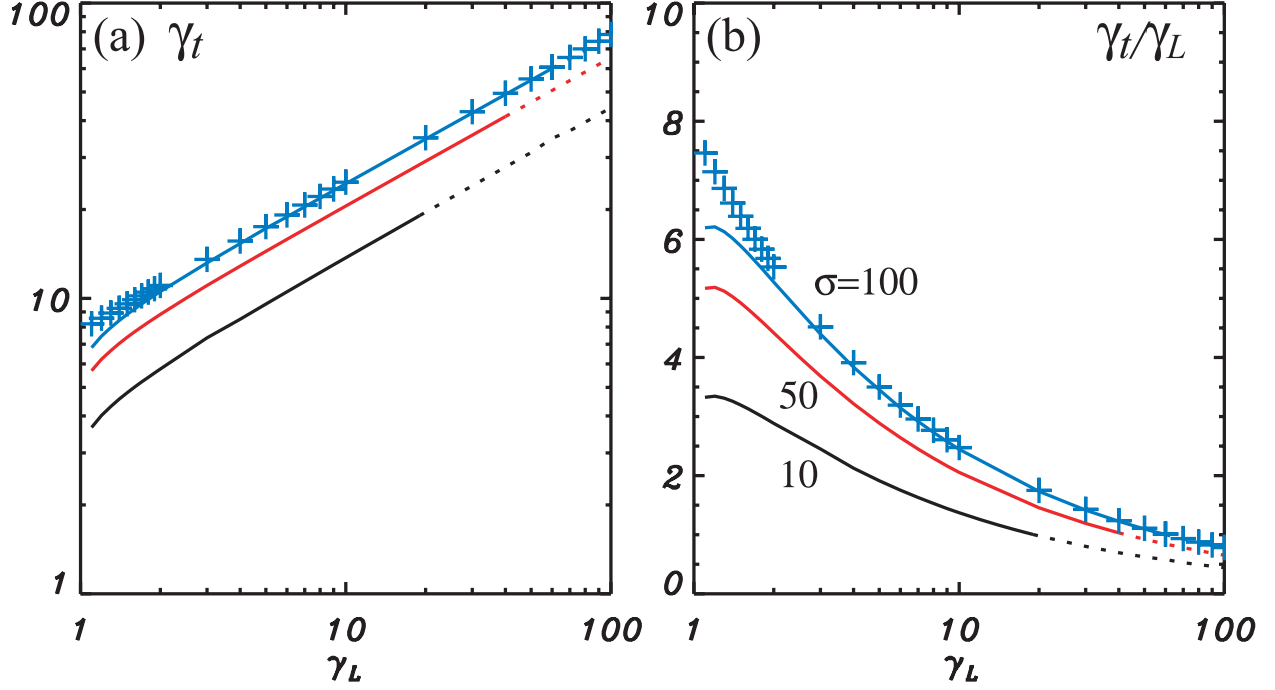


Fig. 3.— The dependences of (a) the terminal Lorentz factor  $\gamma_t$ ; and (2) the acceleration efficiency  $\gamma_t/\gamma_L$  on the initial Lorentz factor  $\gamma_L$ . Solid lines are for the RR regime and dotted lines are for the RS regime. Different initial magnetizations have been calculated:  $\sigma = 10$  (black), 50 (red), and 100 (blue). Crosses are the values of the estimated values based on Eq.(2) for  $\sigma = 100$ .

Numerical MHD simulations (e.g. Koide et al. 1999, 2000; Nishikawa et al. 2005; Mizuno et al. 2007) are essential to understand magnetized relativistic jets. We performed 1-D special relativistic MHD simulations of a relativistic flow propagating in an external medium using the RAISHIN code (Mizuno et al. 2006). The simulation results are in good agreement with the exact solution (Giacomazzo & Rezzolla 2006). This serves as a test of the RAISHIN code. MHD simulations can tackle problems that have no exact solution. We plan to utilize RAISHIN to solve more realistic configurations (e.g., relativistic shells with a finite width and conical geometry, as generally envisaged in the GRB problem).

The magnetic acceleration mechanism discussed here also applies to the Newtonian MHD case. The transition point from a reverse shock to a rarefaction wave is also the pressure balance condition. The terminal velocity of the flow can be estimated from the Newtonian shock jump condition and may be written as  $v_t = c_{s1}(p_2/p_1 - 1)\sqrt{2/\Gamma/[(\Gamma + 1)(p_2/p_1) + (\Gamma - 1)]}$ , where  $c_{s1} = (\Gamma p_1/\rho_1)^{1/2}$  is the sound speed in the upstream medium. This expression is consistent with e.g. Hawley et al. (1984). Defining that  $\sigma = (B_4^2/8\pi)/(\rho_4 v_4^2/2)$  in the Newtonian

case, one can derive the terminal velocity of the flow,  $v_t$  that are determined by the balance between the magnetic pressure and the pressure in the forward shock region. Under this condition, one has  $p_2 = B_3^2/8\pi \simeq B_4^2/8\pi = \sigma\rho_4 v_4^2/2$ . Under the strong shock condition ( $p_2 \gg p_1$ ), the terminal velocity can be roughly written as  $v_t \simeq \sqrt{\sigma(\rho_4/\rho_1)/(\Gamma + 1)}v_4$ . Letting  $v_t = v_4$ , one can derive  $\sigma_c \simeq (\Gamma + 1)\rho_1/\rho_4$ . For  $\Gamma = 5/3$  typical for the non-relativistic shocks, this expression is consistent with Eq.(1) by setting  $\gamma_L = 1$ . We can see that although the general physics is the same, the dependence of the terminal four-velocity  $(v_t/c)\gamma_t$  is different between the Newtonian and the relativistic cases.

Our results have implications for understanding the deceleration of strongly magnetized outflows, which may be present in GRBs and AGNs. Our exact solution indicates that the condition for the existence of a reverse shock is  $\sigma < \sigma_c$ , as suggested by ZK05 (cf. Giannios et al. 2008). The observed paucity of bright optical flashes in GRBs (e.g., Roming et al. 2006) may, among other interpretations, be attributed to highly magnetized flows. Furthermore, the magnetic acceleration mechanism discussed here suggests that  $\sigma$  and  $\gamma$  are not independent parameters at the deceleration radius. For high- $\sigma$  flows, the ejecta would experience magnetic acceleration at small radii, before reaching the coasting regime, so that the coasting Lorentz factor (i.e., the “initial” Lorentz factor for the afterglow) is at least the “terminal” Lorentz factor defined by Eq.(2). As a result, the high- $\sigma$  and low- $\gamma$  part of parameter space is suppressed. This implies that a certain region in the  $\xi - \sigma$  parameter space<sup>3</sup> commonly discussed in GRB models (ZK05; Giannios et al. 2008) is suppressed as well. In this paper we only focus on one-dimensional models with Cartesian geometry. Implications for GRB models will be discussed in more detail when this Riemann problem is solved in conical jet geometry in future work.

Variable TeV emission (down to minute timescales) observed in some TeV blazars suggests very high Lorentz factors in AGN jets (Aharonian et al. 2007). Models for the production of TeV emission have appealed to high Lorentz factor jet cores surrounded by lower Lorentz factor sheaths (Ghisellini et al. 2005) or rapid jet deceleration (Georganopoulos et al. 2005) in order to reconcile the required jet Lorentz factors with lower Lorentz factors suggested by proper motion studies. This study suggests the possibility of magnetic acceleration occurring where highly magnetized jet material overtakes more weakly magnetized jet material. In this case the magnetically accelerated Lorentz factor behind the forward shock can significantly exceed the Lorentz factor of the overtaking jet material.

---

<sup>3</sup> $\xi$  is defined as  $\sqrt{r_{dec}/r_s}$  (Sari & Piran 1995), where  $r_{dec}$  is the deceleration radius defined as the radius where the ejecta accumulate from the external medium a mass  $\gamma_0^{-1}$  times their own mass, and  $r_s$  is the spreading radius where the width of the ejected shell starts to increase due to propagation of a sound wave.

In this paper we only focus on a static unmagnetized medium. In the case of a weakly magnetized medium, all the conclusions presented in this paper still hold.

As a final note of caution, we point out that our calculations/simulations are based on the MHD approximation. The conclusions therefore do not apply to the very large  $\sigma$  regime when the MHD approximation breaks down, e.g.,  $\sigma \sim$  several 100s in the problem of GRBs (Spruit et al. 2001; Zhang & Mészáros 2002).

We thank S. Kobayashi and H. Sol for helpful comments. Y.M. and B.Z. acknowledge NASA NNG05GB67G, NNG05GB68G, and NNX08AE57A for partial support during Y.M.’s stay at UNLV. Y.M., P.H., and K.I.N. acknowledge partial support by NSF AST-0506719, AST-0506666, NASA NNG05GK73G, NNX07AJ88G, and NNX08AG83G. B.G. thanks CSPAR-UAH/NSSTC for hospitality during the preparation of part of this work and acknowledges the DFG grant SFB/Transregio 7 for partial support. S.N. is partially supported by Grants-in Aid for Scientific Research of the Japanese Ministry of Education, Culture, Sports, Science and Technology 19047004, 19104006 and 19740139. The simulations have been performed on Columbia Supercomputer at NAS Division in NASA Ames Research Center and Altix3700 BX2 at YITP in Kyoto University.

## REFERENCES

- Aharonian et al., HESS collaborations, 2007 ApJ, 664, L71
- Aloy, M. A. & Rezzolla, L. 2006, ApJ, 640, L115
- Aloy, M. A. & Mimica, P. 2008, ApJ, 681, 84
- Blandford, R. D. 1976, MNRAS, 176, 465
- Blandford, R. D. & Payne, D. G. 1982, MNRAS, 199, 883
- Blandford, R. D. & Znajek, R. L. 1977, MNRAS, 179, 433
- Fan, Y.-Z., Dai, Z.-G., Huang, Y.-F., & Lu, T. 2002, Ch. J. Astron. Astrophys., 2, 449
- Fan, Y. Z., Wei, D. M., & Wang, C. F. 2004, A&A, 424, 477
- Georganopoulos, M., Perlman, E.S., & Kazanas, D. 2005, ApJ, 634, L33.
- Ghisellini, G., Tavecchio, F., & Chiaberge, M. 2005, A&A, 432, 401

- Giacomazzo, B. & Rezzolla, L. 2006, *J. Fluid Mech.*, 562, 223
- Giannios, D., Mimica, P., & Aloy, M. A. 2008, *A&A*, 478, 747
- Gomboc, A. et al. 2008, *ApJ*, in press, arXiv:0804.1727
- Hardee, P., Mizuno, Y., & Nishikawa, K.-I., 2007, *Ap&SS*, 311, 281
- Hawley, J. F., Smarr, L. L., & Wilson, J. R., 1984, *ApJ*, 277, 296
- Kennel, C. F., & Coroniti, F. V. 1984, *ApJ*, 283, 694
- Kobayashi, S., Piran, T., & Sari, R. 1999, *ApJ*, 513, 669
- Koide, S., Shibata, K., & Kudoh, T. 1999, *ApJ*, 522, 727
- Koide, S., Meier, D. L., Shibata, K., & Kudoh, T. 2000, *ApJ*, 536, 668
- Kumar, P., & Panaitescu, A. 2003, *MNRAS*, 346, 905
- Lovelace, R. V. E. 1976, *Nature*, 262, 649
- Lyutikov, M. 2006, *New J. Phys.*, 8, 119
- Lyutikov, M., & Blandford, R. D. preprint, astro-ph/0312347
- Mészáros, P., & Rees, M. J. 1997, *ApJ*, 482, L29
- Mimica, P., Aloy, M. A., & Müller, E. 2007, *A&A*, 466, 93
- Mimica, P., Giannios, D., & Aloy, M. A. 2008, preprint (arXiv:0801.1325)
- Mizuno, Y., Nishikawa, K.-I., Koide, S., Hardee, P., & Fishman, G. J. 2006, *Proc. VI Microquasar Workshop: Microquasars and Beyond*, ed. Tomaso (Trieste: SISSA), 45
- Mizuno, Y., Hardee, P., Hartmann, D. H., Nishikawa, K.-I., & Zhang, B. 2008, *ApJ*, 672, 72
- Nishikawa, K.-I., Richardson, G., Koide, S., Shibata, K., Kudoh, T., Hardee, P., & Fishman, G. J. 2005, *ApJ*, 625, 60
- Romero, R., Martí, J. M., Pons, J. A., Ibáñez, J. M., & Miralles, J. A. 2005, *J. Fluid Mech.*, 544, 323
- Roming, P. W. A. et al. 2006, *ApJ*, 652, 1416
- Sari, R., & Piran, T. 1995, *ApJ*, 455, L143

- Spruit, H. C., Daigne, F., & Drenkhahn, G. 2001, *A&A*, 369, 694
- Thompson, C. 1994, *MNRAS*, 272, 480
- Usov, V. V. 1992, *Nature*, 357, 472
- Vlahakis, N., & Königl, A. 2003, *ApJ*, 596, 1080
- Vlahakis, N., & Königl, A. 2004, *ApJ*, 605, 656
- Zhang, B., & Kobayashi, S. 2005, *ApJ*, 628, 315 (ZK05)
- Zhang, B., Kobayashi, S., & Mészáros, P. 2003, *ApJ*, 595, 950
- Zhang, B. & Mészáros, P. 2002, *ApJ*, 581, 1236